Splenic Ly6G^{high} mature and Ly6G^{int} immature neutrophils contribute to eradication of *S. pneumoniae*

Justin F. Deniset,[1,3] Bas G. Surewaard,[1,3,4] Woo-Yong Lee,[1,3] and Paul Kubes[1,2,3]

[1]Department of Physiology and Pharmacology, [2]Department of Microbiology, Immunology, and Infectious Diseases, and [3]Snyder Institute for Chronic Diseases, University of Calgary, Calgary, Alberta T2N 4N1, Canada
[4]Department of Medical Microbiology, University Medical Centre, 3584 CX Utrecht, Netherlands

The spleen plays an integral protective role against encapsulated bacterial infections. Our understanding of the associated mechanisms is limited to thymus-independent (TI) antibody production by the marginal zone (MZ) B cells, leaving the contribution of other splenic compartments such as the red pulp (RP) largely unexplored despite asplenic patients succumbing to the infection in the first 24 h, suggesting important antibody-independent mechanisms. In this study, using time-lapse intravital imaging of the spleen, we identify a tropism for *Streptococcus pneumoniae* in this organ mediated by tissue-resident MZ and RP macrophages and a protective role for two distinct splenic neutrophil populations (Ly6G^{hi} and Ly6G^{intermediate}) residing in the splenic RP. Splenic mature neutrophils mediated pneumococcal clearance in the spleen by plucking bacteria off the surface of RP macrophages that caught the majority of bacteria in a complement-dependent manner. This neutrophil phagocytic capacity was further enhanced after TI antibody production. Resident immature neutrophils (Ly6G^{intermediate}) in the spleen undergo emergency proliferation and mobilization from their splenic niche after pneumococcal stimulation to increase the effector mature neutrophil pool. We demonstrate that splenic neutrophils together with two macrophage populations and MZ B cells regulate systemic *S. pneumoniae* clearance through complementary mechanisms.

The Journal of Experimental Medicine

INTRODUCTION

The spleen is important for protection against encapsulated bacteria including *Streptococcus pneumoniae*, a major cause of morbidity and mortality worldwide. Invasive pneumococcal disease, detected in 10–30% of pneumococcal pneumoniae cases, has long been known to increase the mortality substantially beyond that seen with pneumonia alone (Chiou and Yu, 2006; Blasi et al., 2012). It is estimated to directly cause >1.6 million deaths annually (World Health Organization Geneva, 2007; O'Brien et al., 2009). Invasive disease is particularly serious in splenectomized or asplenic patients. These individuals have a 50-fold higher risk of developing a fulminant septic infection to encapsulated bacteria, and a 50–70% mortality rate is associated with these cases (Holdsworth et al., 1991; Di Sabatino et al., 2011). Importantly, the majority of deaths occur within the first 24 h (Gransden et al., 1985; Di Sabatino et al., 2011), highlighting the importance of some very rapid as yet unknown innate immune mechanisms within the spleen in providing protection during the acute stages of i.v. infection before antibody production.

To date, the major protective mechanism of the spleen against *S. pneumoniae* is believed to be dependent on thymus-independent (TI) antibody production by specialized B cells within the marginal zone (MZ). After stimulation, MZ B cells rapidly differentiate into plasmablasts and secrete pathogen-binding serum IgM antibodies that are detectable in the serum only starting at 72–96 h after infection (Martin et al., 2001; Belperron et al., 2005; Moens et al., 2007), meaning other cells must keep the pathogen in check until antibodies are made. Once made, these antibodies are thought to enhance recognition and facilitate clearance of *S. pneumoniae*. Indeed, splenectomized patients display impaired IgM antibody responses to polysaccharide antigen (Amlot and Hayes, 1985; Kruetzmann et al., 2003). As a result, pneumococcal research in the spleen has focused almost exclusively on the cells that regulate B cell–dependent antibody production. However, considering the kinetics of i.v. pneumococcal disease in splenectomized patients, we hypothesize that other very rapid innate immune mechanisms within the spleen must not only contribute to early protection, but also stave off the infection until antibodies can be made.

Neutrophils are first responders in the innate immune response to infection. Their multiple defense mechanisms, such as their phagocytic capacity, reactive oxygen species production, and ability to degranulate and form neutrophil extracellular traps, contribute to the effective clearance of pathogens (Kolaczkowska and Kubes, 2013). Neutrophils typically access sites of infection via the circulation, following

Correspondence to Paul Kubes: pkubes@ucalgary.ca

Abbreviations used: 3D, three dimensional; Cat, cathepsin; CLL, clodronate liposome; IVM, intravital microscopy; MZ, marginal zone; RP, red pulp; SD-IVM, spinning-disk IVM; TI, thymus independent.

The Rockefeller University Press $30.00
J. Exp. Med. 2017 Vol. 214 No. 5 1333–1350
https://doi.org/10.1084/jem.20161621

chemoattractant cues and responding to local inflammatory mediators (Kolaczkowska and Kubes, 2013). In addition to these circulating neutrophils, a large pool of neutrophils can be found in the bone marrow, and marginated pools of neutrophils may also exist within peripheral organs. These sources of neutrophils are thought to mobilize in response to stimulation (Athens et al., 1961a,b). There is some evidence to suggest that the spleen might function as a reservoir. Neutrophils, upon reinjection into humans and mice, appear to accumulate within the spleen (Peters et al., 1985; Ussov et al., 1995; Suratt et al., 2001). Whether this is related to an artifact of neutrophil isolation and reinjection or a bona fide physiological event remains unclear. Recently, a B helper neutrophil subset has been described to reside in the perifollicular zone of the spleen in humans and mice to promote antibody production by MZ B cells (Puga et al., 2012; Magri et al., 2014; Chorny et al., 2016). However, evidence on splenic neutrophil turnover, behavior, and additional functions during basal and infectious conditions is lacking and would require live cell imaging of these cells in the spleen, something that has to date not been done to our knowledge.

In this study, we used a combination of spinning-disk intravital microscopy (IVM [SD-IVM]) and two-photon IVM to evaluate the behavior of neutrophils in the spleen under steady state and after *S. pneumoniae* infection. Using this platform, we found that much but not all of the *S. pneumoniae* bypassed the MZ macrophages and were caught by red pulp (RP) macrophages. We also identified two neutrophil populations within the splenic RP: an immobilized, immature Ly6G-intermediate ($Ly6G^{int}$) population of neutrophils and a mature Ly6G-high ($Ly6G^{hi}$) population of neutrophils that scan the tissue. Mature neutrophils mediated pneumococcal clearance by removing the bacteria from the surface of RP macrophages. During an emergency response to infection, the immobilized $Ly6G^{int}$ immature neutrophils increased their proliferative capacity and took on features of the resident mature neutrophils. Circulating neutrophils recruited to the splenic MZ helped increase TI antibody production by MZ B cells, which further enhanced the ability of mature splenic neutrophils to fully eradicate systemic pneumococcal infection.

RESULTS

The spleen is integral for protection against systemic *S. pneumoniae* infection

A pneumococcal bacteremia model was used to evaluate individual components of immunity during *S. pneumoniae* infection. Intravenous infection with a very small dose (10^4 CFU) of *S. pneumoniae* resulted in a fivefold preferential sequestration by the spleen compared with the lung and liver within 60 min (Fig. 1 a). Bacterial counts in the brain, heart, and kidneys were below detection limit (not depicted). This splenic tropism is unique to *S. pneumoniae* infection, as our previous work has shown tremendous preferential sequestration of circulating *Staphylococcus aureus*, *Escherichia coli*, and *Pseudomonas aeruginosa* by the liver (Kolaczkowska et al., 2015 and unpublished data). In fact, removal of the spleen did not increase blood levels or dissemination of *S. aureus* (unpublished data). The course of *S. pneumoniae* infection was tracked in the spleen and blood over a 5-d period (Fig. 1 b). Bacterial counts decreased in blood and spleen for the first 8 h after infection. This was followed by a rebound in levels at 24 and 48 h before complete clearance by 5 d after infection.

The spleen was integral for clearance, as a pneumococcal challenge in splenectomized mice resulted in 100% mortality by 48 h, even at a fivefold decrease in infection dose (Fig. 1 c). Much focus has been placed on the MZ B cells and MZ macrophages as contributors to antibody production and pneumococcus clearance. Specific depletion of MZ B cells via an antibody-mediated protocol (Lu and Cyster, 2002) resulted in 40% mortality but only in the later phase (72 h) after *S. pneumoniae* infection (Fig. 1 d), coinciding with the MZ B cell–dependent production of IgM and IgG antibodies capable of binding *S. pneumoniae* (Fig. 1 e). Low-dose clodronate liposome (CLL) treatment, which depleted 80–90% of MZ macrophages but not RP macrophages (McGaha et al., 2011), resulted in a nearly identical temporal outcome (Fig. 1 d). Combined MZ macrophage and MZ B cell depletion did not further increase susceptibility to *S. pneumoniae* infection (Fig. 1 d), suggesting a single collaborative protective mechanism of these two cell types via TI antibody production. Importantly, the combined depletion of these two cell populations only partially recapitulated the effect of a splenectomy but with a delayed time frame, indicating that other earlier splenic innate immune mechanisms independent of these two cell types (and their ability to stimulate TI antibody production) are involved in splenic protection to pneumococcus.

S. pneumoniae localizes to both the MZ and the RP of the spleen

Dynamics of *S. pneumoniae* distribution in the spleen were determined using time-lapse two-photon IVM and SD-IVM of the spleen. First, evaluation of *S. pneumoniae* movement in the MZ revealed that, upon i.v. infection, the GFP-expressing bacteria flowed across the MZ, with some tethering interactions to MZ macrophages or other structures in this area (Fig. 2 a and Video 1). Quantification over the first 20 min after infection revealed that the vast majority of bacteria visualized had a short transit time through this area with only a few bacteria (<20%) being detained permanently in the MZ (>5 min in Fig. 2 b). Depletion of MZ macrophages by low-dose CLL treatment resulted in increased localization of bacteria in the RP at 60 min after infection (Fig. 2 c). Visualization of the splenic RP revealed a progressive accumulation of bacteria in this region over the first 20 min (Fig. 2, d and e; and Video 2). RP macrophages are at least in part responsible for this retention, as their depletion through high-dose CLL treatment significantly impaired the number of bacteria in the compartment (Fig. 2 e). This is despite increased bacteria migrating to the RP as a result of the concurrent depletion

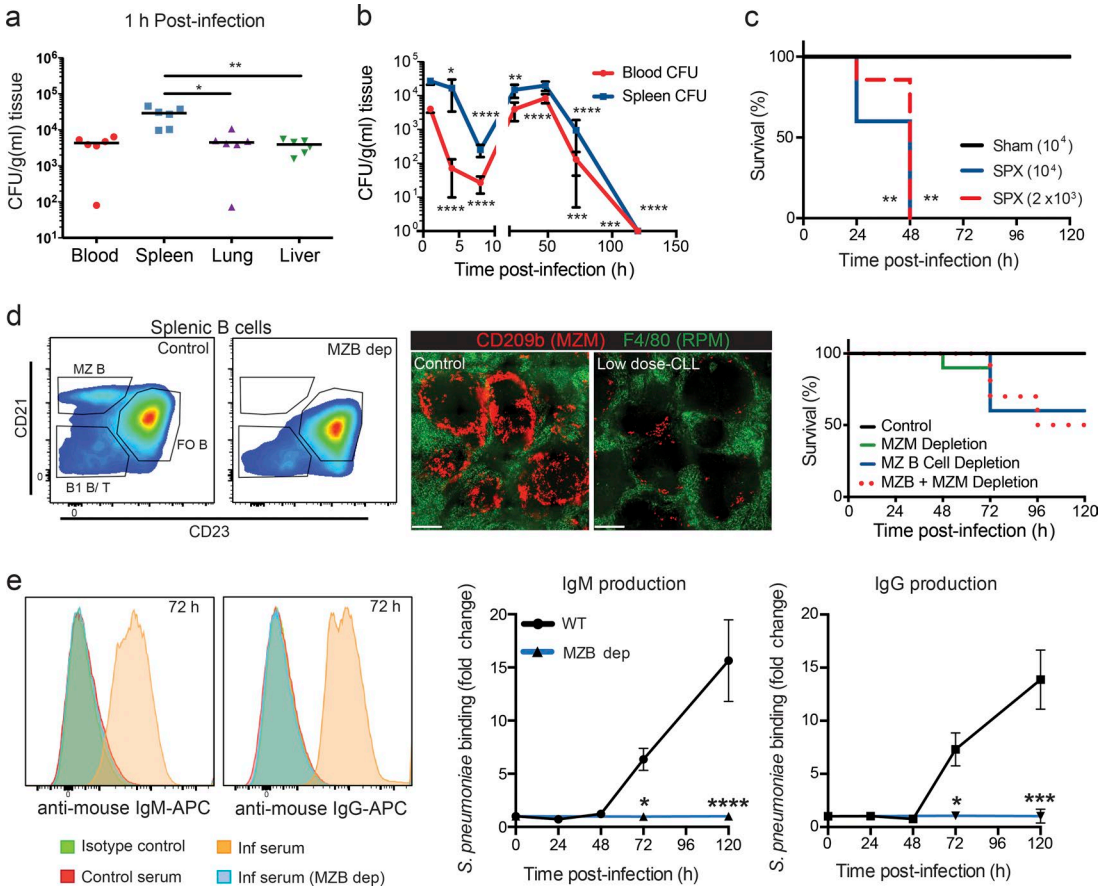

Figure 1. **Splenic protection against *S. pneumoniae* infection.** (a) *S. pneumoniae* bacterial counts in blood, spleen, lung, and liver 1 h after i.v. infection. Black lines show the median. $n = 6$ pooled from two independent experiments. (b) Mean (± SD) bacterial counts in the blood (red circles) and spleen (blue squares) over 120 h. $n = 5–7$ pooled from two independent experiments. (c) Survival curve for *S. pneumoniae* i.v. infection at 10^4-CFU dose in sham-operated (black line) or splenectomized (SPX; solid blue line) mice and at 2×10^3–CFU dose in splenectomized mice (dotted red line). $n = 5$ from one experiment. (d) Representative flow cytometry plots of MZ B cell (MZB) depletion (dep), immunohistochemistry of MZ macrophage (MZM) depletion (green, RP macrophage [RPM]; red, MZ macrophage) and survival curves to *S. pneumonia* infection at 10^4-CFU dose in MZ macrophage–depleted (continuous green line), MZ B cell–depleted (continuous blue line), or MZ macrophage– and MZ B cell–depleted (dotted red line) animals. $n = 6–10$ from two independent experiments. Bar, 300 µm. Fo B, follicular B cell. Histograms and images are representative of two to three independent experiments. (e) Representative flow cytometry histograms and quantification of *S. pneumoniae* IgM (left) and IgG (right) serum antibodies after *S. pneumoniae* infection in WT (orange histogram; black lines) or MZ B cell–depleted *S. pneumoniae* (blue histogram; blue lines) mice. $n = 3$ for WT and $n = 8$ for MZ B cell depletion pooled from three independent experiments. Inf, infected. Data are represented as mean ± SEM, except in b. *, $P < 0.01$; **, $P < 0.01$; ***, $P < 0.001$; ****, $P < 0.0001$. Kruskal-Wallis test (a), one-way ANOVA (b), log-rank Mantel-Cox test (c and d), and two-way ANOVA (e) statistical analyses were performed.

of MZ macrophages. Localization of bacteria in both splenic regions over time was also determined using fresh sections of spleen with labeled RP ($F4/80^+$) and MZ ($CD209b^+$) macrophages. This approach revealed a preferential localization of *S. pneumoniae* in the MZ at 20 min after infection (Fig. 2, f and g), whereas at 1 h after infection, bacteria load increased in the RP (Fig. 2 g).

Flow cytometry was used to identify the main cell types involved in *S. pneumoniae* capture in the spleen. Analysis of splenic *S. pneumoniae*-GFP–positive cells from spleens harvested at 30 min after infection revealed that >60% of bacteria were in populations that resided within the RP of the spleen, whereas MZ macrophages contributed a smaller portion to overall capture (20.1 ± 0.9%; Fig. 2 h). However, RP macrophages only accounted for 18.5 ± 2.1% of the total (Fig. 2 h). Systematic assessment of the remaining population of cells harboring *S. pneumoniae* using flow cytometry revealed that the majority were neutrophils (42 ± 2.9%; Fig. 2 h). The *S. pneumoniae* uptake appeared to be preferential to splenic neutrophils, as the number of total *S. pneumoniae*-GFP–positive neutrophils was significantly higher in the spleen than the blood (Fig. 2 i). Furthermore, neutrophil numbers in the spleen did not increase within the first 30 min after *S. pneumoniae* infection (Fig. 2 j), suggesting that a resident neutrophil population within the spleen is responsible for this bacterial uptake.

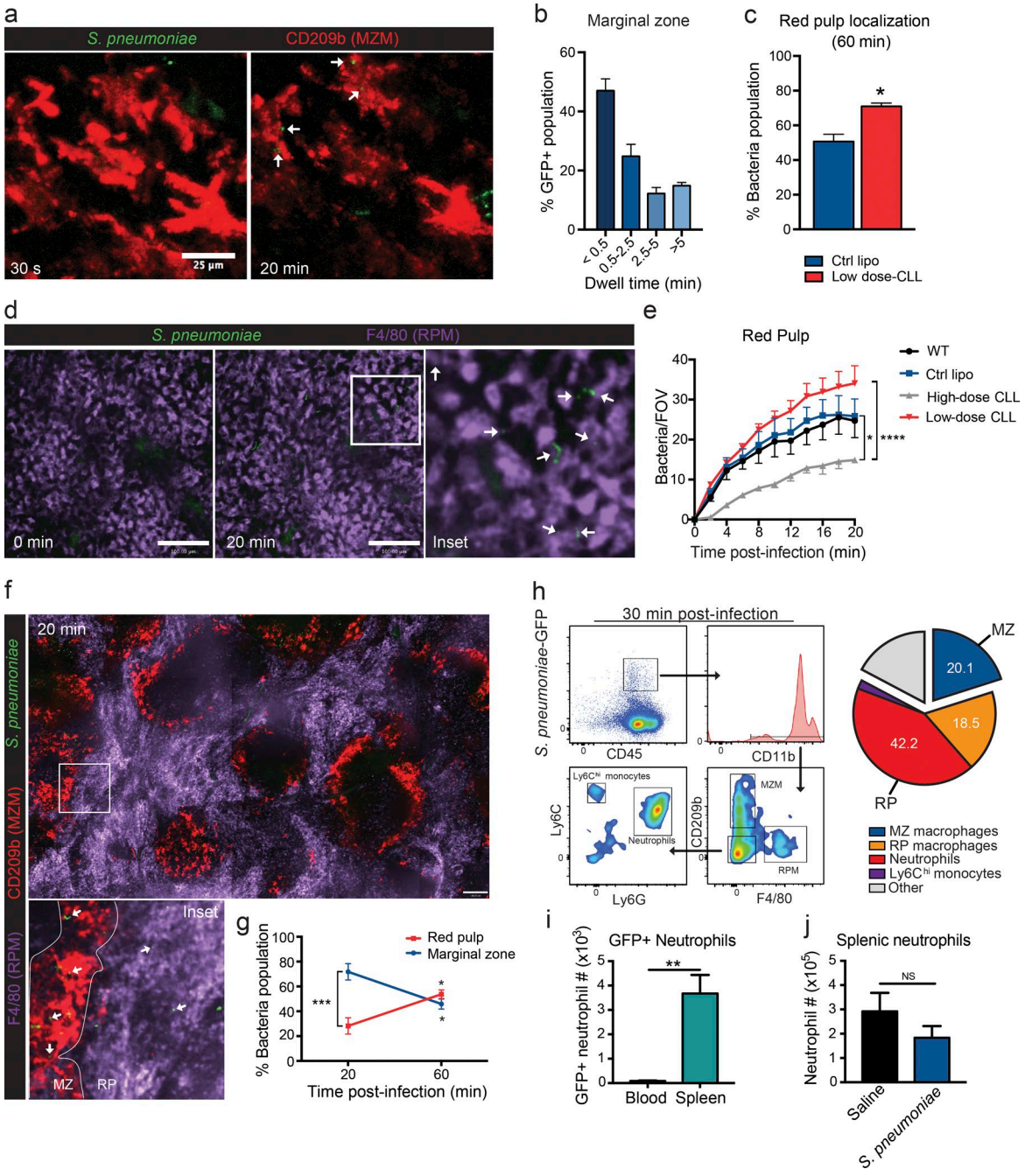

Figure 2. **Splenic localization of *S. pneumoniae*.** (a) Representative two-photon microscopy images of MZ macrophage interaction with *S. pneumoniae* during acute i.v. infection. Bar, 25 µm. Green, *S. pneumoniae*; red, MZ macrophages (MZM). White arrows indicate stationary bacteria. (b) Quantification of MZ dwell time of *S. pneumoniae*. $n = 3$ from three independent experiments. (c) Increased RP localization of *S. pneumoniae* 60 min after i.v. infection in MZ macrophage–depleted (low-dose CLLs; red bar) animals. $n = 3$–4 pooled from two independent experiments. Ctrl lipo, control liposome. (d) Representative spinning-disk confocal images of RP macrophage (RPM) interaction with *S. pneumoniae* during acute i.v. infection. Bars, 100 µm. Green, *S. pneumoniae*; purple, RP macrophages. (Inset) White arrows indicate stationary bacteria. Data are representative of $n = 5$ from three independent experiments. (e) *S. pneumoniae* counts per field of view (FOV) in the RP from 0–20 min after i.v. infection in wild-type (black line), control liposome (blue line)–, low-dose CLL (red line)–, or high-dose CLL (gray line)–treated animals. There were four fields of view per animal. $n = 5$ for WT, $n = 4$ for control liposomes, $n = 3$ for high-dose CLL, and $n = 5$ for low-dose CLL pooled from four independent experiments. (f) Representative composite 10× stitched image of fresh spleen sections at 20 min after i.v. *S. pneumoniae* infection. Bar, 110 µm. Green, *S. pneumoniae*; red, MZ macrophages; purple, RP macrophages. (Inset) White arrows indicate bacteria. (g) Localization of *S. pneumoniae* in both the MZ (blue line) and RP (red line) regions at 20 and 60 min after i.v. infection. $n = 3$ pooled from two independent experiments. (h) *S. pneumoniae* cell localization 30 minutes after infection in the spleen. MZ macrophages, $CD11b^{+}CD209b^{+}F4/80^{-}$; RP macrophages, $CD11b^{low}CD209b^{-}F4/80^{+}$; Neutrophils, $CD11b^{+}Ly6G^{+}Ly6C^{int}$; monocytes, $CD11b^{+}Ly6G^{-}Ly6C^{hi}$. $n = 4$ pooled from two independent experiments.

Neutrophil populations reside in the splenic RP

Time-lapse SD-IVM of the spleen was performed to study resident neutrophils in this organ. Under basal conditions, the spleen contained a large population of neutrophils that were localized in the RP compartment (Video 3). Based on their morphology and behavior, two neutrophil populations could be identified: those that crawled around scanning the tissue (mobile neutrophils) and those that formed large immobile colonies (immobilized neutrophils) that could be as large as 30–50 cells (Fig. 3, a and b). Mobile neutrophils (Fig. 3 a, white arrowheads) migrated throughout the RP at varied velocities (Fig. 3 c), and individual cells could be tracked for up to 1 h within the same field of view (Fig. 3, a–c). Neither of these populations was in the blood vessels. Immobilized neutrophils (Fig. 3 a, green arrowheads) were stationary (Fig. 3 b and Video 3), displayed a rounded morphology, and had a perivascular localization (Fig. 3 a). Aside from these two populations, neutrophils could also be seen rolling within blood vessels, but they rarely stopped, and none emigrated out of the vasculature (Video 3).

To evaluate the turnover of these splenic populations with blood neutrophils, parabiosis experiments pairing a $LysM^{GFP}$ mouse, in which neutrophils express GFP, with a nonfluorescent wild-type mouse (C57) were undertaken. After 2 wk, chimerism within the blood was 20–30%, as determined by flow cytometry (Fig. 3 d), values consistent with that of previous studies (Sawanobori et al., 2008; Guilliams et al., 2013). However, in the spleen, there was a dichotomy. IVM of the spleen in these same animals revealed that 35% of the mobile subset was derived from the parabiotic partner (Fig. 3 d and Video 4), indicating that, under steady state, this population was primarily replenished by neutrophils from the circulation. Interestingly, only 10% of the immobilized clustered neutrophils appeared to derive from the parabiotic partner (Fig. 3 d and Video 4), suggesting the majority of this population was primarily resident.

Intriguingly, analyzing all cells in the spleen, there were clearly two populations of neutrophils: a large population of $Ly6G^{hi}$ neutrophils and a second smaller population of $Ly6G^{int}$ neutrophils. High concentrations of Ly6G (1A8) antibody were given to deplete neutrophils. IVM revealed that all mobile neutrophils were depleted and only immobilized neutrophils remained (Fig. 4 a). Flow cytometric analysis of these spleens revealed a significant decrease in $Ly6G^{hi}$ neutrophils, whereas $Ly6G^{int}$ neutrophils remained unaffected (Fig. 4 a). When spleens from parabiosis animals were examined, the percentage of $Ly6G^{hi}$ neutrophils of partner origin was akin to that of blood overall, whereas the percentage of $Ly6G^{int}$ neutrophils was significantly reduced (Fig. 4 b), suggesting the $Ly6G^{int}$ neutrophils are the resident population. These results support the view that the mobile neutrophils are $Ly6G^{hi}$ and the immobilized resident neutrophils were the $Ly6G^{int}$ population. This was not dissimilar to mature and immature neutrophils, respectively, in bone marrow.

To further characterize whether the $Ly6G^{int}$ neutrophils expressed other markers of immaturity, we examined the expression of c-KIT (CD117) as well as other maturity markers for neutrophils. Expression of CD117 was seen only on $Ly6G^{int}$ neutrophils (Fig. 4 c). CD117 staining was confirmed on immobilized neutrophils by IVM (Fig. 4 d). A portion of clustered $Ly6G^{int}$ neutrophils also displayed increased CD49d (consistent with immature neutrophils) and lower L-selectin expression (Fig. 4 c). No difference was noted in any of the other markers between the two neutrophil populations (Fig. 4 c). Nuclear morphology assessment of immobilized neutrophils in situ demonstrated the presence of banded (Fig. 4 e, white arrowheads) and segmented (Fig. 4 e, blue arrowheads) neutrophils. Collectively, these data further support the view that there are two phenotypically distinct neutrophil populations in the RP, one immature expressing intermediate Ly6G levels and remaining immobilized in large colonies mostly as band cells and a second mature neutrophil population that is Ly6G high and that scans the splenic RP under steady-state conditions.

Mature splenic neutrophils mediate uptake of *S. pneumoniae* in the RP

Next, we examined the behavior of the two populations of neutrophils in the splenic RP by SD-IVM. *S. pneumoniae* uptake by neutrophils in the RP was predominantly limited to mature neutrophils, as the immobilized immature neutrophils bound very little bacteria (Fig. 5, a and b; and Video 5). RP macrophages also bound the bacteria during this time period. Visualization at a higher magnification revealed that *S. pneumoniae* first bound to the surface of an RP macrophage, and the mature neutrophil subsequently migrated over and plucked the bacteria off the macrophage surface (Fig. 5 c and Video 6). At no point were mature neutrophils able to catch *S. pneumoniae* freely flowing in the splenic RP. Three-dimensional (3D) reconstruction of neutrophil-bound bacteria further confirmed intracellular localization of the pathogen. Increasing the transparency of Ly6G staining (Fig. 5 d, I–III) revealed GFP-expressing bacteria. Neutrophil phagocytosis of *S. pneumoniae* was complement dependent, as capture was completely abrogated in C3-deficient mice (Fig. 5 e and Video 5). This was not because of the RP macrophage not being able to catch the bacteria, as the $C3^{-/-}$ RP macrophages caught the *S. pneumoniae*, as well as wild-type

(i) Flow cytometry quantification of total number of *S. pneumoniae*–GFP^+ neutrophils in the blood (black bar) and spleen (teal bar). $n = 4$ pooled from two independent experiments. (j) Flow cytometry quantification of total neutrophil number in the spleen 30 min after saline (black bar) or *S. pneumoniae* (blue bar) injection. $n = 3$ for saline and $n = 4$ for *S. pneumoniae* pooled from two independent experiments. *, $P < 0.01$; **, $P < 0.01$; ***, $P < 0.001$; ****, $P < 0.0001$. Student's *t* test (c, i, and j) and two-way ANOVA (e and g) statistical analyses were performed. Data are represented as mean ± SEM.

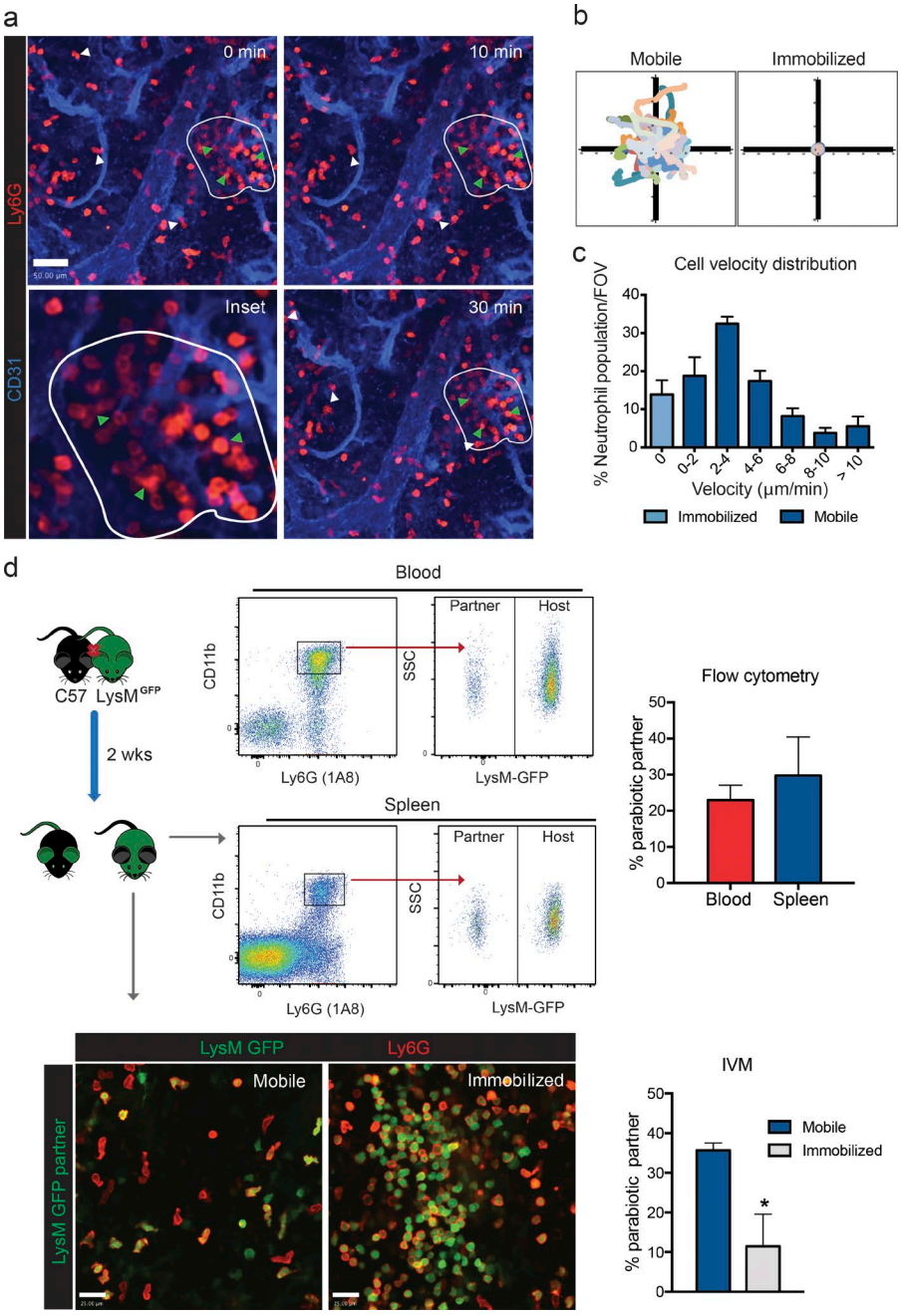

Figure 3. **Steady-state neutrophil populations in the splenic RP.** (a) Representative time-lapse images of mobile (white arrowheads) and immobilized (encircled; green arrowheads) neutrophil populations in the splenic RP under basal conditions. Red, neutrophils; blue, vasculature. Bar, 50 µm. Data are representative of $n = 5$ from three independent experiments. (b) Cellular tracks representation of mobile and immobilized neutrophil populations from representative time-lapse images. (c) Quantification of cell velocity distribution of mobile (dark blue bars) and immobilized (light blue bar) neutrophils in the splenic RP under basal conditions. There were four fields of view (FOV) per animal. $n = 5$ from three independent experiments. (d) Representative flow cytometry plots (blood and spleen), IVM images (spleen), and quantification of neutrophil origin after parabiosis. SSC, side scatter. Bars, 25 µm. There were four fields of view per animal. $n = 4$ from three independent experiments. *, $P < 0.05$. Student's t test statistical analyses were performed. Data are represented as mean ± SEM.

RP macrophages (Fig. 5 e). Intriguingly, in $C3^{-/-}$ mice, where neutrophils were not able to remove the bacteria from the surface of the macrophage, huge numbers of bacteria associated with the RP macrophage and resulted in 100% mortality within the first 18 h of infection (Fig. 5 f). This suggested the macrophages were not able to directly kill the bacteria and required the immediate presence of the neutrophils. Even in the presence of complement, the macrophages were not able to kill bacteria, as depletion of mature neutrophils using a Ly6G (1A8) antibody resulted in increases in splenic bacterial counts at 24 h after infection (Fig. 5 g). Neutrophil-mediated respiratory burst has long been regarded as an important intracellular killing mechanism for pathogens. To evaluate this capacity in mature splenic neutrophils, *S. pneumoniae* was labeled with an OxyBURST probe that fluoresces green in the presence of oxidants. Visualization of OxyBURST-labeled bacteria upon neutrophil phagocytosis demonstrated a very rapid oxidative burst (Fig. 5, h and i). This rapid response was NADPH (nicotinamide adenine dinucleotide phosphate reduced) oxidase dependent, as the oxidant production was not seen in $Cybb^{-/-}$ mice within this timeframe (Fig. 5 i). However, oxidation was not the predominant killing mech-

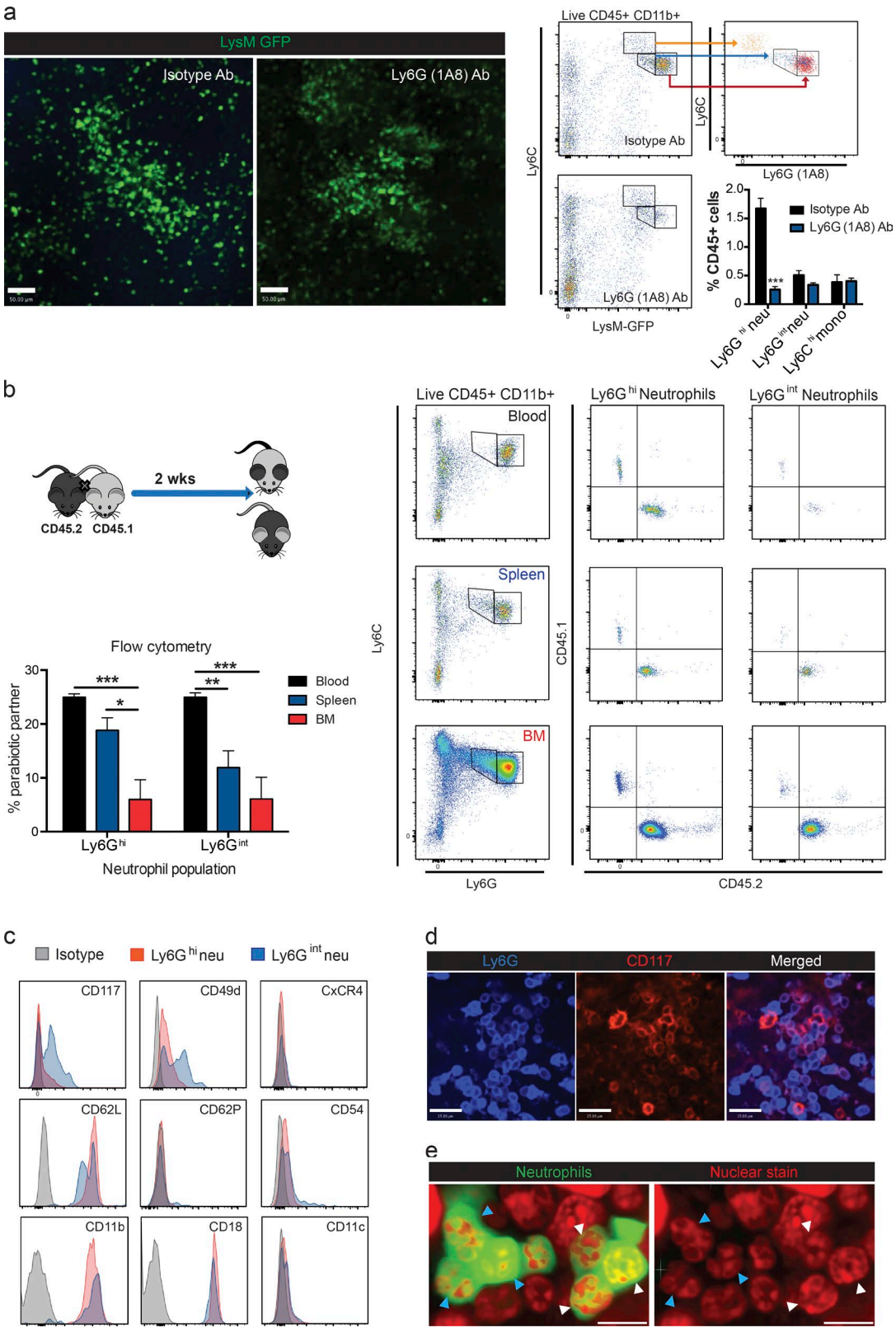

Figure 4. **Characterization of mobile and immobilized splenic neutrophils.** (a) Representative IVM images, flow cytometry plots, and quantification of splenic neutrophils 24 h after administration of isotype antibody (Ab) or Ly6G (1A8) antibody treatment. Green, neutrophils (neu). mono, monocyte. Bars, 50 µm. *n* = 5 for isotype and *n* = 6 for 1A8 antibody pooled from three independent experiments. (b) Representative flow cytometry plots and quantification

anism, as Cybb-deficient animals were able to effectively clear and control the pneumococcal infection (Fig. 5 j). Previous in vitro work with human neutrophils has noted an important contribution of the serine proteases (e.g., cathepsin G [CatG]) and neutrophil elastase in intracellular pneumococcal killing (Standish and Weiser, 2009). In our in vivo model, animals with a deficiency in CatC, a central regulator of serine proteases including CatG and neutrophil elastase, displayed nearly a log-fold increase in mean bacterial load in the spleen, compared with wild-type animals, which was bordering on significant ($P = 0.0628$; Fig. 5 j). A significant difference in bacterial loads was observed between CatC- and Cybb-deficient mice (Fig. 5 j). The increased clearance of *S. pneumoniae* observed in Cybb-deficient animals likely results from increased proteolytic activity that has previously been reported in phagocytes from this mouse strain (Rybicka et al., 2010, 2012). These data suggest an important role for the local mature neutrophils in removing the bacteria from the RP macrophage and helping in bacterial clearance.

Emergency neutrophil maturation occurs in response to *S. pneumoniae*

Neutrophil populations were further evaluated at later time points after infection. Flow cytometric analysis revealed an increase in $Ly6G^{hi}$ neutrophils within the first 24 h after *S. pneumoniae* infection (Fig. 6 a). Conversely, $Ly6G^{int}$ neutrophil numbers did not significantly change within this time period (Fig. 6 a). Although 10% of $Ly6G^{int}$ neutrophils were positive for the proliferative marker Ki67 at baseline, this value increased by 24 h after *S. pneumoniae* administration (Fig. 6 b) and only in the $Ly6G^{int}$ neutrophil population, as none of the $Ly6G^{hi}$ neutrophils were Ki67 positive after infection.

To see whether during infection the immature $Ly6G^{int}$ neutrophils could take on the more mature mobile phenotype, a photoactivatable (UBC-PaGFP) transgenic mouse system was used. This allowed the tracking of the cells over time. When immobilized immature neutrophils were photoactivated under control conditions, ∼10% of the population mobilized over a 1-h period, so now, photoactivatable immobilized GFP-positive neutrophils became GFP-positive mature neutrophils (Fig. 6 c and Video 7), suggesting some immature neutrophils are always maturing in the spleen. After 6-h pneumococcal stimulation, a significantly larger proportion of immobilized progenitor neutrophils were able to start mobilizing and scan the RP over 1 h after photoactivation (Fig. 6 c and Video 7) and contribute to the pool of mature neutrophils within the spleen. Collectively, these data support that proliferation, maturation, and mobilization of the immature $Ly6G^{int}$ into the mature $Ly6G^{hi}$ neutrophil population occurred within the first 24 h after *S. pneumoniae* infection.

Neutrophils from the blood stream are sequestered into the MZ by MZ macrophages and influence TI antibody production

Under basal conditions, very few neutrophils could be found in the MZ. However, at 24 and 48 h after infection, a very dramatic infiltration of neutrophils occurred into the MZ (Fig. 7 a). Two-photon imaging of this area revealed that, after pneumococcal infection, neutrophils leaving the main circulation in the marginal sinus were tethered right out of the mainstream of blood by the MZ macrophages, where they remained rather than moving to the splenic RP (Fig. 7 b). Tracking individual neutrophils in the MZ under basal conditions revealed that the few cells that crawled within the area did so at speeds ranging from 2 to 10 µm/min (Fig. 7 c and Video 8). After the infection, the neutrophils that were recruited from the main stream of blood did not move like the local neutrophils in the RP, but rather, many were not crawling at all at 24 and 48 h after *S. pneumoniae* sequestration in the MZ, and the remainder crawled at the lowest detectable velocity (2–4 µm/s; Fig. 7 c). Indeed, the dwell time (Fig. 7 d) and number of firm interactions of neutrophils with MZ macrophages (Fig. 7 e) were both increased during infections. Depletion of MZ macrophages using low-dose CLL treatment resulted in a significant decrease in MZ localization of neutrophils (Fig. 7 f). These data support a role for MZ macrophages in the retention of splenic neutrophils after pneumococcal infection. Blocking antibodies against various integrins revealed that neutrophil retention in the MZ was partially β1 but not β2 integrin dependent (Fig. 7 g). This decrease in retention could be recapitulated by VCAM-1 blockade (Fig. 7 g), supporting an α4β1–VCAM-1–mediated retention mechanism. It is worth mentioning that other as yet unidentified adhesion molecules make up a significant portion of this retention.

A consequence of this sequestration mechanism into the MZ of the spleen was that the neutrophils localized not only with MZ macrophages, but also with MZ B cells (Fig. 7 h). To see whether this impacted antibody output by these neutrophils, we attempted to deplete neutrophils with Ly6G (1A8) antibody. The results were somewhat ambiguous. Although there was a decreased density of neutrophils in the MZ and RP areas of the spleen after infection (not depicted) when anti-Ly6G was used, the MZ B cell–dependent IgM

of $Ly6G^{hi}$ and $Ly6G^{int}$ neutrophil origin in the blood, spleen, and bone marrow after parabiosis. $n = 4$ from two independent experiments. (a and b) Data are represented as mean ± SEM. *, $P < 0.01$; **, $P < 0.01$; ***, $P < 0.001$. Student's *t* test (a) and one-way ANOVA (b) statistical analyses were performed. (c) Representative flow cytometry histograms of cell-surface marker expression for both $Ly6G^{hi}$ (red) and $Ly6G^{int}$ (blue) neutrophils under steady-state conditions from three independent experiments. (d) Representative immunohistochemistry CD117 staining of the immobilized neutrophil population in the splenic RP from four independent experiments. Bars, 25 µm. (e) Representative nuclear morphology of the immobilized neutrophil population including both banded (white arrowheads) and segmented (blue arrowheads) neutrophils from two independent experiments. Bars, 11.6 µm.

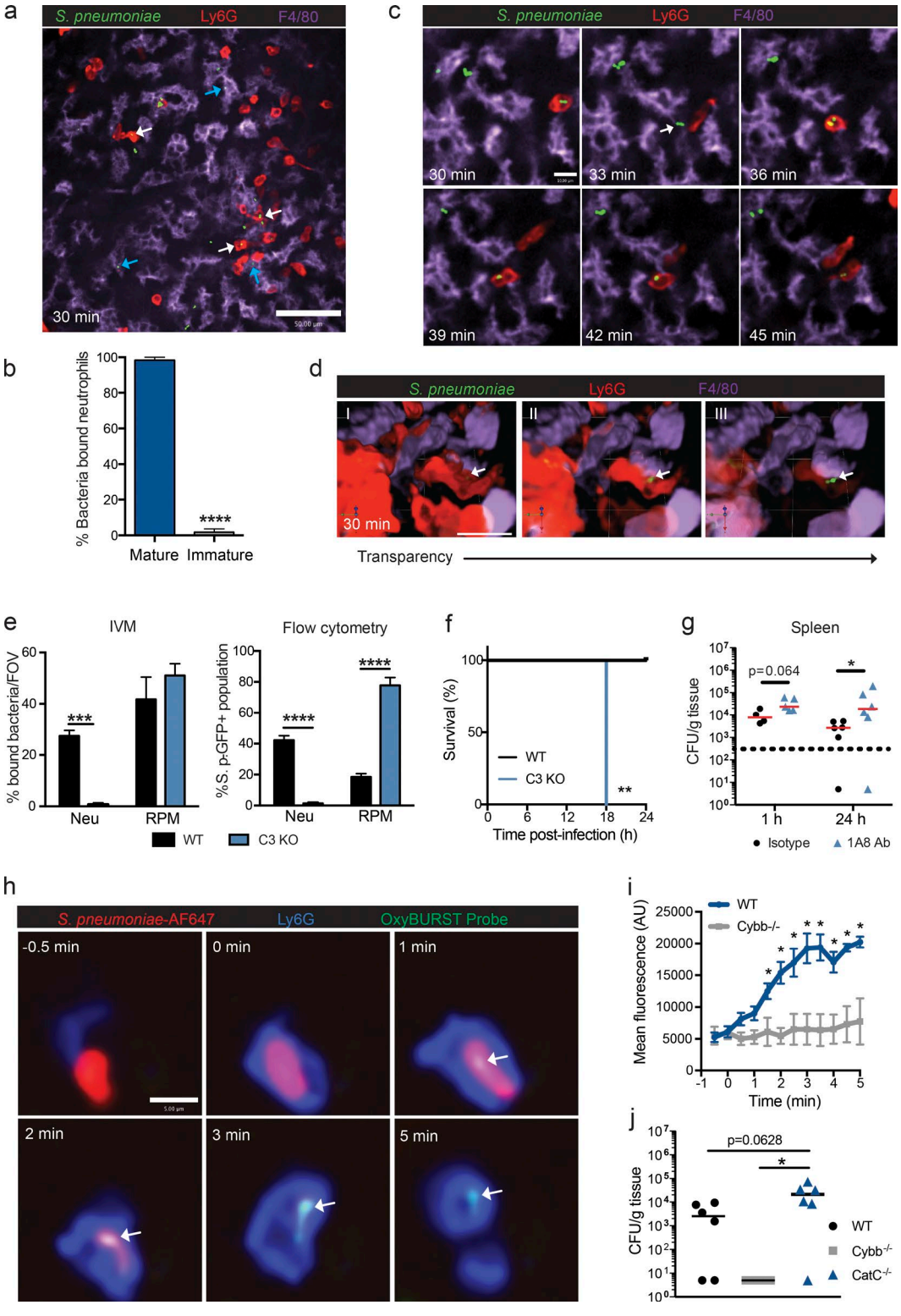

Figure 5. **Mature neutrophil phagocytosis of *S. pneumoniae* in the splenic RP.** (a) Representative spinning-disk confocal image of neutrophils (red) and RP macrophages (purple) containing *S. pneumoniae* (green) at 30 min after infection. Data are representative of $n = 6$ from three independent experiments. Bar, 50 µm. White arrows, bacteria containing neutrophils; blue arrows, bacterial containing RP macrophages. (b) Proportion of splenic neutrophil populations that bound *S. pneumoniae* at 30 min after infection. There were four fields of view per animal. $n = 6$ pooled from three independent experiments. (c) Time-lapse spinning-disk confocal images of *S. pneumoniae* (green) cell adhesion (white arrow) to RP macrophage (purple) and subsequent

and IgG antibody responses occurred in a dichotomous fashion (Fig. 7 i). A portion of the animals displayed low antibody production similar to MZ B cell depletion (Fig. 1 e), whereas normal responses were detected in other animals (Fig. 7 i). It became very clear that although neutrophil depletion efficiency was ∼90% at 24 h, at 72 h it was highly variable in the spleen ranging from as little as 30 to as high as 80%. This likely accounts for much of the antibody variability. Consistent with these data, a similar dichotomy was also observed in both blood and spleen bacterial counts at 72 h after infection (Fig. 7 j). Clearly, the more effective the neutrophil depletion was, the fewer antibodies were produced and the more bacteria were noted. Correlational analysis of these mixed responses revealed that splenic bacterial titers in neutrophil-depleted animals negatively correlated with both IgM ($r = -0.6950$; $P = 0.0402$) and IgG ($r = -0.813$ and $P = 0.0092$) serum antibody levels (not depicted). These data suggest that retained neutrophils in the MZ participate in the TI antibody response after *S. pneumoniae* infection, but one has to be cautious when trying to deplete neutrophils in the spleen long term.

Mature splenic neutrophils mediate TI antibody–dependent pneumococcal clearance

To assess whether MZ B cell–dependent TI antibodies enhanced mature neutrophil function, serum transfer experiments were performed (Fig. 8 a). Transfer of pneumococcus-immunized serum (72 h) resulted in an increased phagocytosis of *S. pneumoniae* by mature neutrophils at 30 min after infection, compared with both control serum (72 h) and pneumococcus-immunized serum from MZ B cell–depleted animals (TI antibody deficient, 72 h; Fig. 8 b). This antibody-dependent mechanism was limited to neutrophils, as no differences in RP macrophage uptake of bacteria were noted between serum transfers (Fig. 8 b). This enhanced neutrophil phagocytic capacity resulted in rapid removal of pneumococcus from the bloodstream (Fig. 8 c). Next, to determine whether these TI antibodies could enhance killing in the absence of the splenic environment, they were injected into splenectomized mice. The data reveal that benefit of the antibodies required splenic neutrophils, as injection of these antibodies into splenectomized mice provided no survival benefit (Fig. 8 d). Collectively, these data highlight the important phagocytic role of mature splenic neutrophils for antibody-mediated clearance of *S. pneumoniae*.

DISCUSSION

This study used imaging to track the dynamic progression of *S. pneumoniae* infection in spleen and has revealed previously unknown mechanisms that increase our understanding of spleen-specific protective mechanisms against this pathogen. This includes the collaboration of local neutrophils and macrophages as early innate immune components in the splenic RP helping to dampen bacterial proliferation. Indeed, we visualized the macrophage of the splenic RP being able to capture and present bacteria to local mature neutrophils. Based on our parabiosis experiments, these local mature neutrophils are recruited constantly from the mainstream of blood under basal conditions. Furthermore, we identify the presence of a second local population of splenic neutrophils that appear to be an immature population that, based on photoactivation experiments, can rapidly mature and mobilize during emergency situations, and this turns out to be key for helping to control the infection until antibodies are made. We also determine the requirement for the TI antibody response by MZ B cells aiding neutrophil phagocytosis for final clearance.

Tissue-resident macrophages play important homeostatic roles including immune surveillance for pathogens. In the context of encapsulated bacterial infection, MZ macrophages have been suggested to be important with their ability to bind the capsule of *S. pneumoniae* via the c-type lectin SIGN-R1 expressed on its surface (Kang et al., 2004). Our data support this work but also provide new information on a second population of splenic macrophages, the RP macrophages, which appear to contribute in a major way to initial binding and tropism of *S. pneumoniae* to the spleen. This macrophage function appears to be limited to the spleen, as Kupffer cells in the liver were less effective at catching encap-

phagocytosis by neutrophils (red). Data are representative of $n = 4$ from three independent experiments. Bar, 10 µm. (d) 3D reconstruction of intracellular *S. pneumoniae* (green) within neutrophil (red) at 30–60 min after infection. Transparency of neutrophils is increased from left to right. Bar, 23.3 µm. Data are representative of $n = 3$ from two independent experiments. White arrows indicate intracellular bacteria. (e) IVM and flow cytometric quantification of *S. pneumoniae* phagocytosis by neutrophils (Neu) and RP macrophages (RPM) from 30–60 min after i.v. infection in wild-type (black bars) and C3-deficient (blue bars) animals. $n = 3$–6 pooled from three and two independent experiments for IVM and flow cytometry, respectively. FOV, field of view; S. p., *S. pneumoniae*. (f) Survival curve for *S. pneumoniae* i.v. infection at 10^4-CFU dose in wild-type (black line) or C3 KO (blue line) mice. $n = 5$ from one experiment. (g) *S. pneumoniae* bacterial counts in the spleen at 1 and 24 h after i.v. infection in isotype antibody (black circles)– and Ly6G (1A8) antibody (1A8 Ab; blue triangles)–treated animals. $n = 4$–6 pooled from two independent experiments. Red lines show the median. (h) Time-lapse spinning-disk confocal images of OxyBURST probe activation (green) after *S. pneumoniae* (red) phagocytosis by mature splenic neutrophil (blue). Data are representative of $n = 6$ from two independent experiments. Bar, 5 µm. White arrows indicate OxyBURST activation on the surface of intracellular bacteria. (i) Quantification of intracellular OxyBURST probe activation within neutrophils in wild-type (blue line) and $Cybb^{-/-}$ (gray line) mice. $n = 3$–6 pooled from two independent experiments. AU, arbitrary units. (j) *S. pneumoniae* bacterial counts in the spleen at 24 h after i.v. infection in wild-type (black circles), $Cybb^{-/-}$ (gray squares), and $CatC^{-/-}$ (blue triangles) animals. $n = 4$–6 pooled from two independent experiments. Black lines show the median. *, $P < 0.01$; **, $P < 0.01$; ***, $P < 0.001$; ****, $P < 0.0001$. Student's *t* test (b, e, and i), log-rank Mantel-Cox test (f), and Mann-Whitney test (g and j) statistical analyses were performed. Data are represented as mean ± SEM.

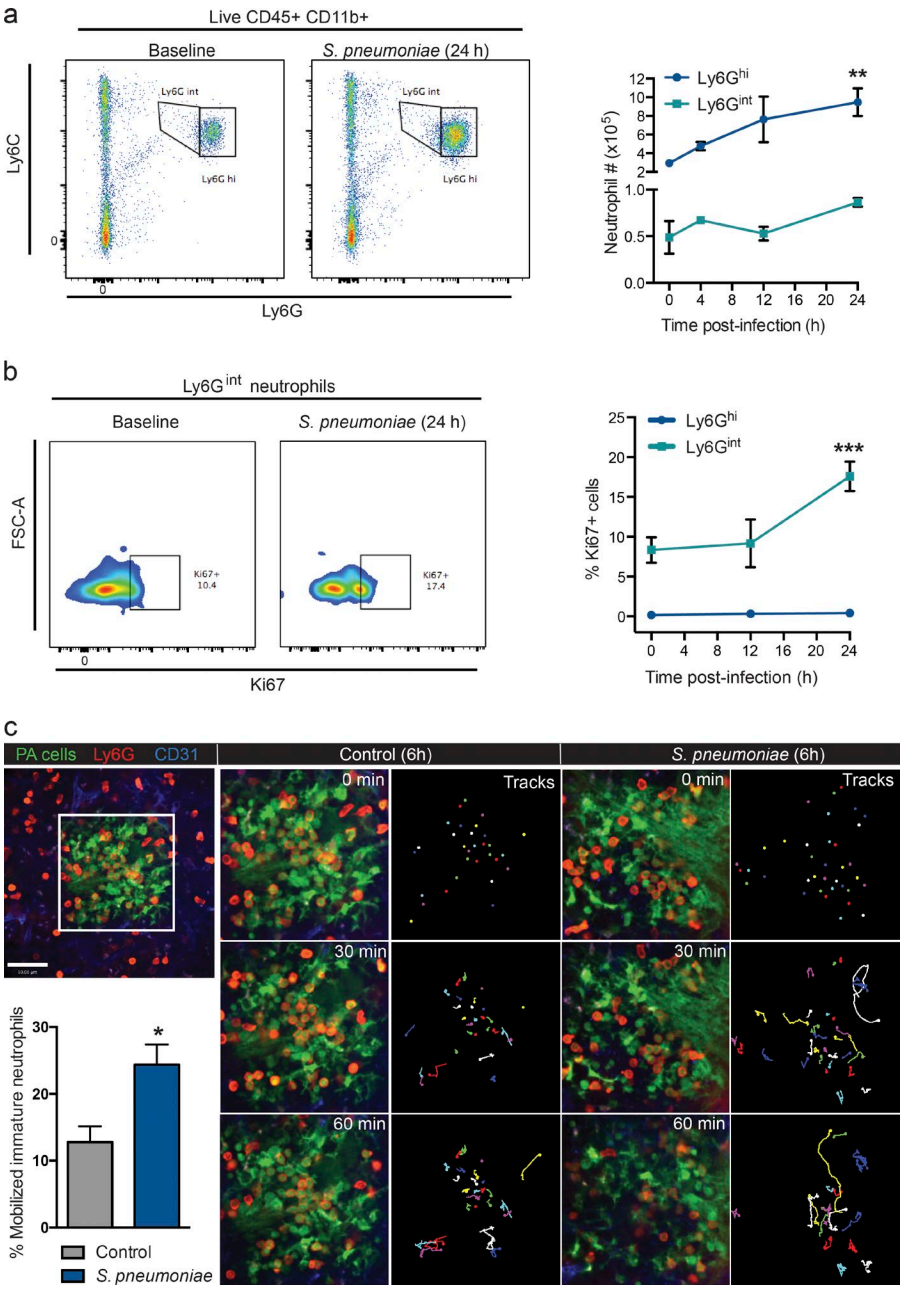

Figure 6. **Splenic immature neutrophil proliferation and mobilization after pneumococcal stimulation.** (a) Representative flow cytometry plots (baseline and 24 h) and quantification of Ly6G^{hi} (blue line) and Ly6G^{int} (teal line) neutrophil populations at baseline and after *S. pneumoniae* infection. n = 4–6 pooled from four independent experiments. **, $P < 0.01$ versus 0 h (baseline). (b) Representative flow cytometry histograms and quantification of Ki67 staining in both Ly6G^{hi} (blue line) and Ly6G^{int} (teal line) neutrophil populations at baseline and after *S. pneumoniae* infection. Positive gates were established by use of an AF488-conjugated isotype control within each experiment. n = 3–4 pooled from two independent experiments. ***, $P < 0.001$ versus 0 and 12 h. FSC, forward scatter. (c) Time-lapse (0–60 min) spinning-disk confocal images of photoactivated neutrophil cluster mobilization (top left, white box) in the splenic RP at 6 h after saline (gray bar) or *S. pneumoniae* (blue bar) administration. Green, photoactivated (PA) cells; red, neutrophils; blue, vasculature; multicolored, tracks. Bar, 50 µm. n = 4 pooled from four independent experiments. *, $P < 0.05$. One-way ANOVA (a and b) and Student's t test (c) statistical analyses were performed. Data are represented as mean ± SEM.

sulated *S. pneumoniae* in the sinusoidal circulation (unpublished data). Although both splenic macrophage populations sequestered pneumococcus early, they contributed to *S. pneumoniae* infection defense by distinct mechanisms. MZ macrophages contributed to TI antibody production by MZ B cells, consistent with another study (Koppel et al., 2008). This is likely by facilitating the direct interaction of MZ B cells with the pathogen on the surface of the macrophages and indirectly enhancing MZ B cell activation through recruitment of neutrophils at the MZ. Interestingly, MZ macrophages displayed only a small amount of catching of *S. pneumoniae* as observed by intravital imaging. In fact, RP macrophages had a larger contribution to initial binding and subsequent clearance of *S. pneumoniae* mediated by mature neutrophils. RP macrophage binding of *S. pneumoniae* in our model was not dependent on complement and was not enhanced with passive immunization, suggesting an alternative mechanism.

In addition to resident macrophages, the spleen also serves as an important reservoir for other myeloid cells. Swirski et al. (2009) described a pool of monocytes that reside within the RP under steady-state conditions and that can be mobilized to the sites of injury. We demonstrate that mature neutrophils are also present within the RP compartment under basal conditions and carry out an important fil-

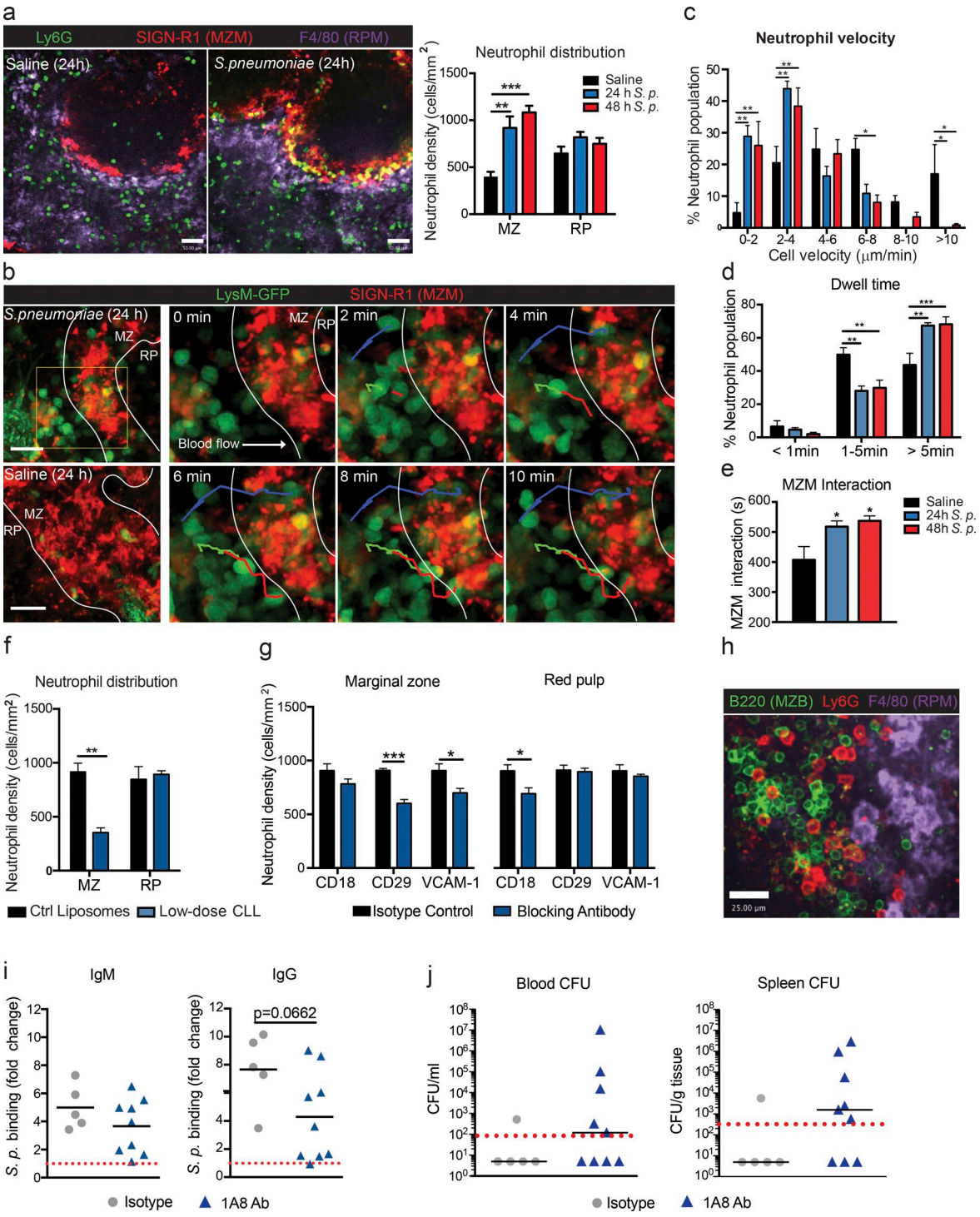

Figure 7. **Neutrophil sequestration by MZ macrophages contributes to TI antibody response after pneumococcal infection.** (a) Representative confocal images and quantification of neutrophil (green) colocalization with MZ macrophages (MZM; red) and RP macrophages (RPM; purple) after saline (black bars) or *S. pneumoniae* (*S. p.*; 24 h, blue bars; 48 h, red bars) i.v. injection. Bars, 50 µm. Eight fields of view were averaged per animal. $n = 4–6$ pooled from four independent experiments. (b) Time-lapse two-photon microscopy images of neutrophil behavior in MZ 24 h after *S. pneumoniae* injection. Green, neutrophils; red, MZM; multicolored, tracks. Bars, 25 µm. (c–e) Tracking quantification of neutrophil cell velocity (c), dwell time (d), and MZ macrophage interaction time (e) at 24 h (blue bars) and 48 h (red bars) after *S. pneumoniae* i.v. infection. Two fields of view were averaged per animal. $n = 3–4$ pooled from four independent experiments. (f) Quantification of neutrophil colocalization with MZ B cells and RP macrophages at 24 h after *S. pneumoniae* i.v. infection in control (Ctrl) liposomes and low-dose CLL–treated animals. $n = 3–5$ pooled from three independent experiments. (g) Quantification of neutrophil

tering function within the organ by mediating phagocytosis of bacteria. This protective mechanism is not restricted to encapsulated bacteria, as phagocytosis of *S. aureus* and *Listeria monocytogenes* has also been observed with our system (unpublished data), supporting an immune surveillance role for this pool of neutrophils. The spleen also has the capacity to increase both neutrophil and monocyte numbers by facilitating extramedullary hematopoiesis during inflammation (Swirski et al., 2009; Robbins et al., 2012). This is thought to occur by mobilization of hematopoietic stem and progenitor cells from the bone marrow to the spleen, where they seed preestablished niches and undergo expansion (Swirski et al., 2009). Intriguingly, the recently described hematopoietic niche in the splenic RP (Dutta et al., 2015; Inra et al., 2015) shares common features with the local environment surrounding our described Ly6G^{int} immature neutrophils, including the perivascular location and the presence of VCAM-1–positive macrophages around the colonies (unpublished data). It is likely that our immature neutrophils represent the consequence of continuous extramedullary hematopoiesis during the steady state, albeit at a very slow rate. Upon inflammatory stimulation, these immature neutrophils can mobilize as observed and contribute to the mature neutrophil population.

Neutrophils in the spleen have previously been shown to contribute to MZ B cell activation and subsequent production of anti-capsular polysaccharide antibodies (Puga et al., 2012; Magri et al., 2014; Chorny et al., 2016). Pentraxin 3 has recently been identified as a natural adjuvant produced and released by these B helper neutrophils to help mediate this response (Chorny et al., 2016). Although, some have not been able to confirm these observations in humans (Nagelkerke et al., 2014), our data does support a role for newly recruited splenic neutrophils in promoting anti-pneumococcal TI antibody production during systemic mouse pneumococcal infection. Although it is very easy to deplete circulating neutrophils to determine their function, the resident mature population in the spleen was extremely difficult to eradicate during infection, and the immature population was resistant to 1A8 depletion. In fact, similar depletion inefficiency of splenic neutrophils has previously been noted in a chronic inflammatory setting of tumor-bearing mice (Moses et al., 2016). It was unclear whether this resident population could impact on B cell antibody production. Nevertheless, in those mice where we obtained good depletion, we also got better inhibition of antibody production and increased bacterial load, consistent with a potential role for regulation of antibody production by neutrophils within the spleen.

Although most tissues rely on circulating neutrophils for recruitment, the spleen appeared to compartmentalize its recruitment; in the MZ, there was classical recruitment of neutrophils from the vasculature, whereas the RP had its own population of immature and mature neutrophils that were key for local eradication of *S. pneumoniae*. The obvious advantage of this type of system is that, at the first sign of infection, neutrophils are already in the RP ready to help kill bacteria caught by the macrophage. Without the neutrophils there, the bacteria were able to increase their numbers dramatically within the spleen, killing the host. Although at this point we can only conclude that it is the immediate presence of neutrophils in spleen that helped to eradicate bacteria, an additional possibility is that the circulating neutrophils that enter the RP further mature to perform a necessary function that circulating neutrophils are incapable of doing. In fact, under steady-state conditions, we do note a more activated phenotype for mature splenic neutrophils compared with circulating neutrophils (unpublished data). Many of these features are reminiscent of B helper neutrophils, which are proposed to polarize locally in response to bacterial factors and GM-CSF, which is released locally by innate lymphoid cells (Magri et al., 2014; Chorny et al., 2016). It will also be interesting to know whether during systemic infections such as sepsis, where most neutrophils are recruited to lungs and other infectious sites and in some instances patients become neutropenic, this local pool helps to maintain neutrophil presence in the spleen for critical innate immune purposes.

MATERIALS AND METHODS

Animals

8–12-wk-old male and female mice were used for experiments. C57BL/6, Pep BoyJ(B6), LysM-eGFP/eGFP, UBC-PaGFP, and Cybb-deficient (Cybb$^{-/-}$) mice were obtained from The Jackson Laboratory, and CatC-deficient (CatC$^{-/-}$) mice were a gift from GlaxoSmithKline. All mice were housed under a specific pathogen–free, double-barrier unit at the University of Calgary. Mice were fed autoclaved rodent feed and water ad libitum. All protocols used were in accordance with the guidelines drafted by the University of Calgary Animal Care Committee and the Canadian Council on the Use of Laboratory Animals.

colocalization with MZ B cells (left) and RP macrophages (right) at 24 h after *S. pneumoniae* i.v. infection in animals treated with isotope control, anti-CD18, anti-CD29, and anti–VCAM-1 blocking antibodies. Eight fields of view were averaged per animal. n = 3–5 pooled from three independent experiments. (h) Representative image of neutrophil localization within the MZ B cells (MZB) 24 h after i.v. *S. pneumoniae* infection. Green, MZ B cells; red, neutrophils; purple, RP macrophages. Data are representative of n = 4 from two independent experiments. Bar, 25 µm. (i) Quantification of *S. pneumoniae*–specific serum IgM and IgG antibody levels in isotype antibody–treated and Ly6G (1A8) antibody (1A8 Ab)–treated animals at 72 h after infection. Red dotted lines indicate antibody levels in MZ B cell–depleted animals. n = 5–9 total pooled from three independent experiments. (j) *S. pneumoniae* bacterial counts in the blood and spleen at 72 h after i.v. infection in isotype antibody–treated and Ly6G (1A8) antibody–treated animals. Black lines show the median, and red dotted lines show the detection limit. n = 5–9 total pooled from three independent experiments. *, $P < 0.05$; **, $P < 0.01$; ***, $P < 0.001$. One-way ANOVA (a and e), two-way ANOVA (c and d), Student's t test (f, g, and i), and Mann-Whitney test (j) statistical analyses were performed.

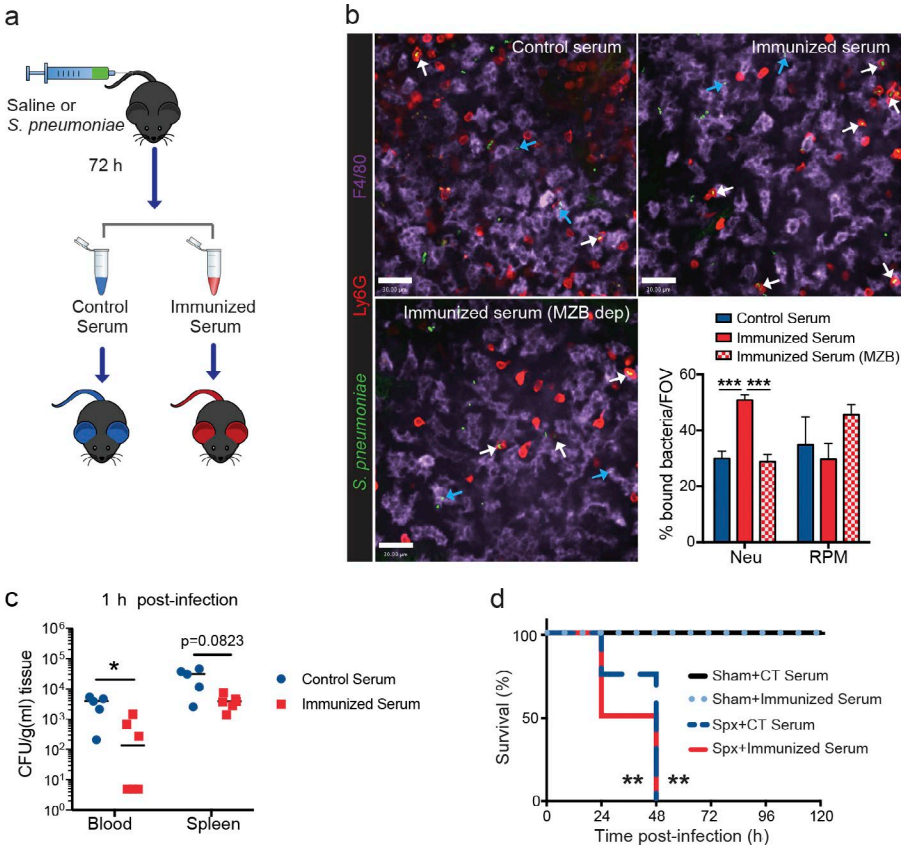

Figure 8. **Passive immunization facilitates neutrophil-mediated capture and clearance of *S. pneumoniae* in the spleen.** (a) Schematic of serum transfer protocol. (b) Representative spinning disk confocal images and quantification of neutrophils (Neu; red) and RP macrophages (RPM; purple) containing *S. pneumoniae* (green) at 30–60 min after infection in animals given control serum (blue bars), immunized serum (solid red bars), and immunized serum from MZ B cell–depleted (MZB dep) animals (checkered red bars). Bars, 30 µm. White arrows indicate neutrophil containing bacteria, and blue arrows indicate RP macrophage containing bacteria. Eight fields of view (FOV) were averaged per animal. n = 3–4 pooled from two independent experiments. Data are represented as mean ± SEM. (c) *S. pneumoniae* bacterial counts in the blood and spleen at 1 h after i.v. infection in wild-type mice receiving either control serum (blue circles) or immunized serum (red squares). n = 5–6 pooled from two independent experiments. (d) Survival curve to *S. pneumoniae* infection at 10^4-CFU dose in sham-operated and splenectomized (Spx) animals receiving control (CT) serum or immunized serum. n = 4–5 from one experiment. *, $P < 0.05$; **, $P < 0.01$; ***, $P < 0.001$. One-way ANOVA (b), Mann-Whitney test (c), and Log-rank Mantel-Cox test (d) statistical analyses were performed.

IVM

Multichannel spinning-disk confocal and two-photon confocal microscopes were used to image mouse spleens. Mice were anaesthetized (10 mg/kg xylazine hydrochloride and 200 mg/kg ketamine hydrochloride). The right jugular vein was cannulated to administer fluorescent dyes and additional anesthetic. After skin incision, the mouse was placed in a left lateral position, and the spleen was exteriorized onto a glass coverslip on the inverted microscope stage. The stage was kept at 37°C to maintain the mouse body temperature.

Image acquisition of the splenic RP was performed using an inverted microscope (IX81; Olympus), equipped with a focus drive (Olympus) and a motorized stage (Applied Scientific Instrumentation) and fitted with a motorized objective turret equipped with 4×/0.16 UPLANSAPO, 10×/0.40 UPLANSAPO, and 20×/0.70 UPLANSAPO objective lenses and coupled to a confocal light path (WaveFx; Quorum Technologies) based on a modified CSU-10 head (Yokogawa Electric Corporation). Cells of interest were visualized using fluorescently labeled antibodies, fluorescent reporter mice, and fluorescent reporter bacteria. Typically, RP macrophages and neutrophils were stained by i.v. injection of 2.5 µg anti–F4-80 and 1 µg anti-Ly6G fluorescent conjugated mAbs, respectively. Laser excitation wavelengths of 491, 561, 642, and 730 nm (Cobolt) were used in a rapid succession together with the appropriate band-pass filters (Semrock). A back-thinned electron-multiplying charge-coupled device 512 × 512–pixel camera (Hamamatsu Photonics) was used for fluorescence detection. Volocity software (PerkinElmer) was used to drive the confocal microscope and for 3D rendering, acquisition, and analysis of images. Bacteria and neutrophil behavior was evaluated using Volocity software. Both populations were identified and tracked using the Find Object and Track functions, respectively, within the measurement modality. For each animal, tracking data were averaged for multiple fields of view and considered an n = 1.

Image acquisition of the splenic MZ was performed using an inverted multiphoton microscope (TCS SP8; Leica Biosystems) or upright multiphoton microscope (TCS SP8; Leica Biosystems). Typically, MZ macrophages were stained by i.v. injection of 1 µg anti-CD209b fluorescent conjugated mAbs. i.v. injection of 2 µg anti-MARCO (macrophage receptor with collagenous structure) fluorescent conjugated mAbs was also used to label MZ macrophages in preliminary experiments to confirm that 1 µg anti-CD209b did not affect *S. pneumoniae* binding. The dynamic behaviors of immune cells and bacteria were visualized simultaneously with a single-pulsed laser (Ti-Sapphire; Spectra-Physics or Coherent) at 950 nm or 1,040 nm in combination with appropriate band-pass emission filters (Semrock). The fluorescence was detected

by HyD hybrid or high-sensitivity photomultiplier non-descanned detectors. Leica Biosystems software was used to drive the confocal microscope and for 3D rendering and acquisition of images. Files were converted from LIF format into multiple TIFFs using Volocity and subsequently imported into ImageJ (National Institutes of Health) for analysis. The plugin StackReg was used for movement correction purposes. Both bacteria and neutrophil tracking were completed using the Manual Tracking plugin. For each animal, tracking data were averaged for multiple images and considered an $n = 1$. For photoactivation experiments, multiphoton excitation at 800 nm was used to activate neutrophil populations of interest, and images were acquired using a spinning-disk microscope as described in the previous paragraph.

Parabiosis

Age-matched female mice were housed together for 2 wk before surgery. Parabiotic pairs of mice were generated surgically as previously described (Ajami et al., 2007). In brief, a skin incision running from elbow to knee along the flank was generated on opposite sides of the mice to be paired. The mice were first joined with a suture through the shoulder and thigh muscles, and next, the inside faces of the skin flaps were juxtaposed and sutured. Complete blood sharing was monitored between 12 and 17 d by tail vein blood sampling. 24 h after chimerism detection in the blood, pairs were separated and prepared for subsequent intravital imaging of the spleen and/or flow cytometry of the spleen, blood, and bone marrow.

Bacterial growth and infection

The *S. pneumoniae* D39-GFP strain was grown on blood agar plates overnight at 37°C with 95% O_2/5% CO_2. Single colonies were picked from plates and grown in brain-heart infusion broth at 37°C with CO_2 until an OD 600 of 0.5 was reached. Bacteria were resuspended in saline and diluted to achieve appropriate dose with a 100-µl volume. For long-term infection and acute bacteria infection, doses of 2×10^3 CFU or 10^4 CFU and 5×10^6 CFU were administered i.v., respectively. Generation of reporter bacteria for oxidation was performed as previously described (Surewaard et al., 2016). In brief, fresh streptococcal cultures were washed twice in saline, resuspended at 5×10^8 CFU in 500 µl in carbonate, pH 8.3, buffered saline, and labeled for 30 min with 20 µg ml^{-1} AF647 *N*-hydroxysuccinimide ester (Thermo Fisher Scientific) and 60 µg ml^{-1} OxyBURST Green H2DCFDA SE (DMSO stock; Thermo Fisher Scientific) under vigorous agitation. Activation of OxyBURST was accomplished by adding 250 µl of 1.5 M hydroxylamine, pH 8.5, and incubating for 30 min on ice. Reporter bacteria were washed twice with PBS and injected i.v. into mice at 5×10^6–10^7 CFU.

Bacteriological analysis

Anesthetized mice were washed with 70% ethanol under aseptic conditions. Blood was collected in a heparinized syringe by cardiac puncture. The lungs, liver, heart, kidneys, and spleen were removed after thoracotomy, weighed, and homogenized. For determination of CFUs, 50 µl of blood and 100 µl of tissue homogenate were serially diluted, plated onto blood agar plates, and incubated at 37°C with 5% CO_2 for 18 h, and bacterial colonies were counted.

Serum antibody measurement

Blood was collected by cardiac puncture at multiple time points after either saline or *S. pneumoniae* injection and spun down at 400 *g* for 10 min. Then, serum was collected, and 25 µl was diluted with an equal volume of FACS wash buffer (1× PBS, 2% FBS, and 0.2% EDTA) and subsequently incubated with 10^6 CFU of freshly cultured *S. pneumoniae* for 30 min on ice. After a wash step, 1 µg of APC-conjugated anti–mouse IgG or IgM antibody was added in a resuspension volume of 50 µl and incubated for an additional 30 min. Antibody concentration used was determined by a preliminary serial dilution experiment to ensure optimal signal saturation. Samples were subsequently fixed with 0.5% paraformaldehyde in flow cytometry wash buffer and run using a flow cytometer (LSRII; BD). Samples were first gated on GFP^+ bacteria, and then, the median fluorescence intensities were determined for APC-labeled anti-IgG or IgM. Values were normalized to control animal (saline injected) levels within each experiment and then averaged among multiple experiments.

Serum transfer experiments

Serum was collected as described in the previous paragraph at 72 h after injection (saline or *S. pneumoniae*). After confirmation of antibody production, serum from multiple animals (same treatment) was combined and heat inactivated at 56°C for 20 min. 100 µl of the control, immunized, or immunized (MZ B cell depletion) heat-inactivated serum was administered i.v. 20–30 min before infection with *S. pneumoniae*.

Flow cytometry

Mice were anesthetized, and the spleen was removed and placed in PBS on ice. Then, blood was collected in a heparinized syringe by cardiac puncture. The spleen was passed through a 70-µm filter. For *S. pneumoniae*–GFP^+ detection experiments, cells were immediately stained for 20 min with fluorescently labeled antibodies and subsequently incubated in 1× Fix/Lyse buffer (eBioscience). For the remainder of experiments, residual red blood cells were lysed using ACK lysing buffer (Invitrogen). The cells were blocked using anti-CD16/32 antibody (2.4G2 clone; Bio X Cell) for 20–30 min. Then, cells were stained for 30 min with specified markers including FITC-labeled B220 (RA3-6B2; BD), CD18 (C71/16; BD), CD62P (RB40.3; BD), CD45.2 (104; BD), CD43 (eBioR2/60; eBioscience), PE-labeled anti–mouse Ly6G (1A8; eBioscience), F4/80 (BM8; eBioscience), CD 21/35 (4E3; eBioscience), CD117 (2B8; eBioscience), CD49d (R1-2; eBioscience), CxCR4 (2B11; eBioscience), CD62L (MEL-14; eBioscience), CD169 (3D6.112; BioLegend), APC-labeled anti–mouse CD209b (22D1; eBioscience),

CD23 (B3B4; eBioscience), CD45.1 (A20; eBioscience), PerCP Cy5.5-labeled Ly6C (HK 1.4; eBioscience), PE-Cy7–labeled CD11b (M1/70; eBioscience), Pacific blue–labeled Ly6G (1A8; eBioscience), AF647-labeled CD54 (YN1/1.7.4; BioLegend), efluor 660–labeled CD11c(N418; eBioscience), Brilliant violet 510–labeled CD45 (30-F11; BioLegend), and APC-Cy7–labeled CD45 (30-F11; eBioscience). Appropriate isotype control antibodies were used to confirm positive signals. Nonviable cells were identified using propidium iodide or viability dye efluor 780 (eBioscience). Samples were run using a flow cytometer (FACSCanto; BD) and analyzed using FlowJo software (Tree Star). Neutrophils were identified as $CD11b^{+}$ $Ly6G^{hi}$ $Ly6C^{int}$ or LysM GFP^{hi} SSC^{hi} (for depletion experiments). Proinflammatory monocytes were identified as $CD11b^{+}$ $Ly6G^{-}$ $Ly6C^{hi}$. RP macrophages were identified as $CD11b^{+/lo}$ $CD209b^{-}$ $F4/80^{hi}$. MZ macrophages were identified as $CD11b^{+}$ $CD209b^{hi}$ $F4/80^{-}$. Metallophilic macrophages were identified as $CD11b^{+}$ $CD169^{+}$ $F4/80^{-/lo}$. Follicular B cells were identified as $B220^{+}$ $CD23^{hi}$ $CD21/35^{int}$, MZ B cells as $B220^{+}$ $CD23^{lo}$ $CD21/35^{int/hi}$, and B1 B cells as $B220^{+}$ $CD23^{lo}$ $CD21/35^{lo}$ $CD43^{+}$.

Depletion and blocking antibody protocols

Depletion protocols for various cell types have been used as previously described (Lu and Cyster, 2002; McGaha et al., 2011; Kolaczkowska et al., 2015). In brief, transient MZ B cell depletion was achieved by intraperitoneal injection of 100 µg of both anti-CD11a (M17/4; Bio X Cell) and anti-CD49d (PS/2; Bio X Cell) 96 h before *S. pneumoniae* infection. Depletion of MZ macrophages was completed by i.v. delivery of a low-dose clodronate treatment (100 µg) 96 h before infection. Neutrophils were depleted using an anti-Ly6G (1A8; Bio X Cell) antibody. For acute infection experiments, a single 500-µg dose was given intraperitoneally 24 h before infection. For long-term infection, supplemental 200-µg doses were given daily. Isotype antibodies or control liposomes were given as control injections. The specificity of all three depletion protocols was verified using both flow cytometry and in some instances immunohistochemistry. LysM-GFP reporter mice for our depletion studies were used to evaluate neutrophil depletion. $Ly6G^{hi}$ neutrophils were identified as $Ly6C^{int}$ GFP^{hi}, $Ly6G^{int}$ neutrophils as $Ly6C^{int}$ GFP^{int}, and $Ly6C^{hi}$ monocytes as $Ly6C^{hi}$ GFP^{int}. These gates were established in experiments performed with control and isotype antibody–treated LysM-GFP mice with the inclusion of the Ly6G antibody (1A8 clone).

For blocking antibody experiments, 100 µg of purified anti-CD18 (clone M18/2; BioLegend), anti-CD29 (clone HMβ1-1; BioLegend), or anti-CD106 (clone 429; eBioscience) was added i.v. 10 min before *S. pneumoniae* infection. Appropriate isotype control antibodies were used for control experiments.

Statistical analysis

Statistical comparisons were performed using Prism (v6.0; GraphPad Software). Data are represented as mean ± SEM unless otherwise specified. Data, with the exception of bacterial CFUs, were compared either by unpaired two-tailed Student's *t* test or one-way or two-way ANOVA followed by Bonferroni posthoc test for multiple comparisons adjustment. Bacterial CFU data were compared by Mann-Whitney test or Kruskal-Wallis test followed by Dunn's multiple comparisons test. Survival curves were compared using log-rank (Mantel-Cox) test. Statistical significance was set at $P < 0.05$. The applied statistical analyses and the numbers of independent replicates (*n*) are reported in the figure legends.

Online supplemental material

Video 1 displays the movement of *S. pneumoniae* in the splenic MZ after infection. Video 2 shows *S. pneumoniae* accumulation in the splenic RP after infection. Video 3 demonstrates in vivo behavior of splenic neutrophil populations under steady-state conditions. Video 4 shows chimerism of both mature and immature splenic neutrophils after parabiosis. Video 5 displays in vivo capture of *S. pneumoniae* by splenic neutrophils in the presence or absence of complement. Video 6 shows neutrophil-mediated removal and phagocytosis of *S. pneumoniae* after initial binding to RP macrophages. Video 7 shows mobilization of photoactivated immature neutrophils after *S. pneumoniae* infection. Video 8 displays the in vivo behavior of circulating neutrophils in the splenic MZ.

ACKNOWLEDGMENTS

We thank Trecia Nussbaumer and Dr. Robin Yates for the breeding of mice. We thank Dr. Craig Jenne and Dr. Bryan Yipp for use of their multiphoton microscopes. We thank Dr. Pina Colarusso at the Snyder Live Cell Imaging Facility for technical support for photoactivation experiments and Dr. Karen Poon (Snyder Institute Molecular Core) for assistance with flow cytometry.

P. Kubes is supported by a foundation grant from the Canadian Institutes of Health Research and a Heart and Stroke Foundation of Canada grant. J.F. Deniset is financially supported by a postgraduate fellowship from Alberta Innovates–Health Solutions. B.G. Surewaard is partially funded by Marie Curie Actions (FP7-PEOPLE-2013-IOF; grant no. 627575) and a postgraduate fellowship from Alberta Innovates–Health Solutions.

The authors declare no competing financial interests.

Author contributions: J.F. Deniset and B.G. Surewaard conceived the study, performed experiments, analyzed data, and wrote the manuscript. W.-Y. Lee contributed to parabiosis experiments. P. Kubes wrote the manuscript and directed the study.

Submitted: 27 September 2016

Revised: 27 January 2017

Accepted: 3 March 2017

REFERENCES

Ajami, B., J.L. Bennett, C. Krieger, W. Tetzlaff, and F.M. Rossi. 2007. Local self-renewal can sustain CNS microglia maintenance and function throughout adult life. *Nat. Neurosci.* 10:1538–1543. http://dx.doi.org/10.1038/nn2014

Amlot, P.L., and A.E. Hayes. 1985. Impaired human antibody response to the thymus-independent antigen, DNP-Ficoll, after splenectomy: Implications for post-splenectomy infections. *Lancet.* 325:1008–1011. http://dx.doi.org/10.1016/S0140-6736(85)91613-7

Athens, J.W., O.P. Haab, S.O. Raab, A.M. Mauer, H. Ashenbrucker, G.E. Cartwright, and M.M. Wintrobe. 1961a. Leukokinetic studies. IV. The total blood, circulating and marginal granulocyte pools and the granulocyte turnover rate in normal subjects. *J. Clin. Invest.* 40:989–995. http://dx.doi.org/10.1172/JCI104338

Athens, J.W., S.O. Raab, O.P. Haab, A.M. Mauer, H. Ashenbrucker, G.E. Cartwright, and M.M. Wintrobe. 1961b. Leukokinetic studies. III. The distribution of granulocytes in the blood of normal subjects. *J. Clin. Invest.* 40:159–164. http://dx.doi.org/10.1172/JCI104230

Belperron, A.A., C.M. Dailey, and L.K. Bockenstedt. 2005. Infection-induced marginal zone B cell production of *Borrelia hermsii*-specific antibody is impaired in the absence of CD1d. *J. Immunol.* 174:5681–5686. http://dx.doi.org/10.4049/jimmunol.174.9.5681

Blasi, F., M. Mantero, P. Santus, and P. Tarsia. 2012. Understanding the burden of pneumococcal disease in adults. *Clin. Microbiol. Infect.* 18:7–14. http://dx.doi.org/10.1111/j.1469-0691.2012.03937.x

Chiou, C.C., and V.L. Yu. 2006. Severe pneumococcal pneumonia: new strategies for management. *Curr. Opin. Crit. Care.* 12:470–476.

Chorny, A., S. Casas-Recasens, J. Sintes, M. Shan, N. Polentarutti, R. García-Escudero, A.C. Walland, J.R. Yeiser, L. Cassis, J. Carrillo, et al. 2016. The soluble pattern recognition receptor PTX3 links humoral innate and adaptive immune responses by helping marginal zone B cells. *J. Exp. Med.* 213:2167–2185. http://dx.doi.org/10.1084/jem.20150282

Di Sabatino, A., R. Carsetti, and G.R. Corazza. 2011. Post-splenectomy and hyposplenic states. *Lancet.* 378:86–97. http://dx.doi.org/10.1016/S0140-6736(10)61493-6

Dutta, P., F.F. Hoyer, L.S. Grigoryeva, H.B. Sager, F. Leuschner, G. Courties, A. Borodovsky, T. Novobrantseva, V.M. Ruda, K. Fitzgerald, et al. 2015. Macrophages retain hematopoietic stem cells in the spleen via VCAM-1. *J. Exp. Med.* 212:497–512. http://dx.doi.org/10.1084/jem.20141642

Gransden, W.R., S.J. Eykyn, and I. Phillips. 1985. Pneumococcal bacteraemia: 325 episodes diagnosed at St Thomas's Hospital. *Br. Med. J. (Clin. Res. Ed.).* 290:505–508. http://dx.doi.org/10.1136/bmj.290.6467.505

Guilliams, M., I. De Kleer, S. Henri, S. Post, L. Vanhoutte, S. De Prijck, K. Deswarte, B. Malissen, H. Hammad, and B.N. Lambrecht. 2013. Alveolar macrophages develop from fetal monocytes that differentiate into long-lived cells in the first week of life via GM-CSF. *J. Exp. Med.* 210:1977–1992. http://dx.doi.org/10.1084/jem.20131199

Holdsworth, R.J., A.D. Irving, and A. Cuschieri. 1991. Postsplenectomy sepsis and its mortality rate: actual versus perceived risks. *Br. J. Surg.* 78:1031–1038. http://dx.doi.org/10.1002/bjs.1800780904

Inra, C.N., B.O. Zhou, M. Acar, M.M. Murphy, J. Richardson, Z. Zhao, and S.J. Morrison. 2015. A perisinusoidal niche for extramedullary haematopoiesis in the spleen. *Nature.* 527:466–471. http://dx.doi.org/10.1038/nature15530

Kang, Y.S., J.Y. Kim, S.A. Bruening, M. Pack, A. Charalambous, A. Pritsker, T.M. Moran, J.M. Loeffler, R.M. Steinman, and C.G. Park. 2004. The C-type lectin SIGN-R1 mediates uptake of the capsular polysaccharide of *Streptococcus pneumoniae* in the marginal zone of mouse spleen. *Proc. Natl. Acad. Sci. USA.* 101:215–220. http://dx.doi.org/10.1073/pnas.0307124101

Kolaczkowska, E., and P. Kubes. 2013. Neutrophil recruitment and function in health and inflammation. *Nat. Rev. Immunol.* 13:159–175. http://dx.doi.org/10.1038/nri3399

Kolaczkowska, E., C.N. Jenne, B.G. Surewaard, A. Thanabalasuriar, W.Y. Lee, M.J. Sanz, K. Mowen, G. Opdenakker, and P. Kubes. 2015. Molecular mechanisms of NET formation and degradation revealed by intravital imaging in the liver vasculature. *Nat. Commun.* 6:6673. http://dx.doi.org/10.1038/ncomms7673

Koppel, E.A., M. Litjens, V.C. van den Berg, Y. van Kooyk, and T.B. Geijtenbeek. 2008. Interaction of SIGNR1 expressed by marginal zone macrophages with marginal zone B cells is essential to early IgM responses against *Streptococcus pneumoniae*. *Mol. Immunol.* 45:2881–2887. http://dx.doi.org/10.1016/j.molimm.2008.01.032

Kruetzmann, S., M.M. Rosado, H. Weber, U. Germing, O. Tournilhac, H.H. Peter, R. Berner, A. Peters, T. Boehm, A. Plebani, et al. 2003. Human immunoglobulin M memory B cells controlling *Streptococcus pneumoniae* infections are generated in the spleen. *J. Exp. Med.* 197:939–945. http://dx.doi.org/10.1084/jem.20022020

Lu, T.T., and J.G. Cyster. 2002. Integrin-mediated long-term B cell retention in the splenic marginal zone. *Science.* 297:409–412. http://dx.doi.org/10.1126/science.1071632

Magri, G., M. Miyajima, S. Bascones, A. Mortha, I. Puga, L. Cassis, C.M. Barra, L. Comerma, A. Chudnovskiy, M. Gentile, et al. 2014. Innate lymphoid cells integrate stromal and immunological signals to enhance antibody production by splenic marginal zone B cells. *Nat. Immunol.* 15:354–364. http://dx.doi.org/10.1038/ni.2830

Martin, F., A.M. Oliver, and J.F. Kearney. 2001. Marginal zone and B1 B cells unite in the early response against T-independent blood-borne particulate antigens. *Immunity.* 14:617–629. http://dx.doi.org/10.1016/S1074-7613(01)00129-7

McGaha, T.L., Y. Chen, B. Ravishankar, N. van Rooijen, and M.C. Karlsson. 2011. Marginal zone macrophages suppress innate and adaptive immunity to apoptotic cells in the spleen. *Blood.* 117:5403–5412. http://dx.doi.org/10.1182/blood-2010-11-320028

Moens, L., A. Jeurissen, G. Wuyts, P.G. Fallon, B. Louis, J.L. Ceuppens, and X. Bossuyt. 2007. Specific intracellular adhesion molecule-grabbing nonintegrin R1 is not involved in the murine antibody response to pneumococcal polysaccharides. *Infect. Immun.* 75:5748–5752. http://dx.doi.org/10.1128/IAI.00574-07

Moses, K., J.C. Klein, L. Männ, A. Klingberg, M. Gunzer, and S. Brandau. 2016. Survival of residual neutrophils and accelerated myelopoiesis limit the efficacy of antibody-mediated depletion of Ly-6G$^+$ cells in tumor-bearing mice. *J. Leukoc. Biol.* 99:811–823. http://dx.doi.org/10.1189/jlb.1HI0715-289R

Nagelkerke, S.Q., D.J. aan de Kerk, M.H. Jansen, T.K. van den Berg, and T.W. Kuijpers. 2014. Failure to detect functional neutrophil B helper cells in the human spleen. *PLoS One.* 9:e88377. http://dx.doi.org/10.1371/journal.pone.0088377

O'Brien, K.L., L.J. Wolfson, J.P. Watt, E. Henkle, M. Deloria-Knoll, N. McCall, E. Lee, K. Mulholland, O.S. Levine, and T. Cherian. Hib and Pneumococcal Global Burden of Disease Study Team. 2009. Burden of disease caused by *Streptococcus pneumoniae* in children younger than 5 years: global estimates. *Lancet.* 374:893–902. http://dx.doi.org/10.1016/S0140-6736(09)61204-6

Peters, A.M., S.H. Saverymuttu, A. Keshavarzian, R.N. Bell, and J.P. Lavender. 1985. Splenic pooling of granulocytes. *Clin. Sci.* 68:283–289. http://dx.doi.org/10.1042/cs0680283

Puga, I., M. Cols, C.M. Barra, B. He, L. Cassis, M. Gentile, L. Comerma, A. Chorny, M. Shan, W. Xu, et al. 2012. B cell–helper neutrophils stimulate the diversification and production of immunoglobulin in the marginal zone of the spleen. *Nat. Immunol.* 13:170–180. http://dx.doi.org/10.1038/ni.2194

Robbins, C.S., A. Chudnovskiy, P.J. Rauch, J.L. Figueiredo, Y. Iwamoto, R. Gorbatov, M. Etzrodt, G.F. Weber, T. Ueno, N. van Rooijen, et al. 2012. Extramedullary hematopoiesis generates Ly-6C^{high} monocytes that infiltrate atherosclerotic lesions. *Circulation.* 125:364–374. http://dx.doi.org/10.1161/CIRCULATIONAHA.111.061986

Rybicka, J.M., D.R. Balce, M.F. Khan, R.M. Krohn, and R.M. Yates. 2010. NADPH oxidase activity controls phagosomal proteolysis in macrophages through modulation of the lumenal redox environment of phagosomes. *Proc. Natl. Acad. Sci. USA.* 107:10496–10501. http://dx.doi.org/10.1073/pnas.0914867107

Rybicka, J.M., D.R. Balce, S. Chaudhuri, E.R. Allan, and R.M. Yates. 2012. Phagosomal proteolysis in dendritic cells is modulated by NADPH

oxidase in a pH-independent manner. *EMBO J.* 31:932–944. http://dx.doi.org/10.1038/emboj.2011.440

Sawanobori, Y., S. Ueha, M. Kurachi, T. Shimaoka, J.E. Talmadge, J. Abe, Y. Shono, M. Kitabatake, K. Kakimi, N. Mukaida, and K. Matsushima. 2008. Chemokine-mediated rapid turnover of myeloid-derived suppressor cells in tumor-bearing mice. *Blood.* 111:5457–5466. http://dx.doi.org/10.1182/blood-2008-01-136895

Standish, A.J., and J.N. Weiser. 2009. Human neutrophils kill *Streptococcus pneumoniae* via serine proteases. *J. Immunol.* 183:2602–2609. http://dx.doi.org/10.4049/jimmunol.0900688

Suratt, B.T., S.K. Young, J. Lieber, J.A. Nick, P.M. Henson, and G.S. Worthen. 2001. Neutrophil maturation and activation determine anatomic site of clearance from circulation. *Am. J. Physiol. Lung Cell. Mol. Physiol.* 281:L913–L921.

Surewaard, B.G.D., J.F. Deniset, F.J. Zemp, M. Amrein, M. Otto, J. Conly, A. Omri, R.M. Yates, and P. Kubes. 2016. Identification and treatment of the *Staphylococcus aureus* reservoir in vivo. *J. Exp. Med.* 213:1141–1151. http://dx.doi.org/10.1084/jem.20160334

Swirski, F.K., M. Nahrendorf, M. Etzrodt, M. Wildgruber, V. Cortez-Retamozo, P. Panizzi, J.L. Figueiredo, R.H. Kohler, A. Chudnovskiy, P. Waterman, et al. 2009. Identification of splenic reservoir monocytes and their deployment to inflammatory sites. *Science.* 325:612–616. http://dx.doi.org/10.1126/science.1175202

Ussov, W.Y., C. Aktolun, M.J. Myers, F. Jamar, and A.M. Peters. 1995. Granulocyte margination in bone marrow: comparison with margination in the spleen and liver. *Scand. J. Clin. Lab. Invest.* 55:87–96. http://dx.doi.org/10.3109/00365519509075382

World Health Organization Geneva. 2007. Pneumococcal conjugate vaccine for childhood immunization—WHO position paper. *Wkly. Epidemiol. Rec.* 82:93–104.